Redox and magnetic switching in 1,3,5-acceptor-substituted benzenes: reversible formation of radical anions, dianions and trianions in doublet, triplet, and quartet spin states

Ernst Beer,[a] Jörg Daub,*[a] Cornelia Palivan[b] and Georg Gescheidt*[b]

[a] *Institute of Organic Chemistry, Universität Regensburg, Universitätsstrasse 31, D-93053 Regensburg, Germany. E-mail: joerg.daub@chemie.uni-regensburg.de*
[b] *Department of Chemistry, Universität Basel, Klingelbergstrasse 80, CH-4056 Basel, Switzerland. E-mail: georg.gescheidt@unibas.ch*

Received (in Cambridge, UK) 8th March 2002, Accepted 18th June 2002
First published as an Advance Article on the web 17th July 2002

1,3,5-Tris(dicyanovinyl)-substituted benzene **1** can accept one, two, and three electrons stepwise, as shown by (spectro)electrochemical methods. When the corresponding redox stages are attained by K-metal reduction in THF and 2-methyltetrahydrofuran, paramagnetic resonance and optical techniques can identify equilibria between adjacent redox states and different (para)magnetic stages. It can be shown that the dianion can adopt a triplet state whereas the trianion is present in a doublet and quartet spin multiplicity. Similar findings are established for the methoxy-substituted derivative **2**. The formation of the different paramagnetic stages is closely connected to the association of the anions with alkali-metal countercations.

Introduction

1,3,5-Trisubstituted benzenes (**A**) have served as successful prototypes for the development of organic magnets. The threefold *meta*-substitution pattern promotes the formation of high-spin states at the molecular level. Several molecules of this type have been described, *e.g.*, neutral radicals like Schlenk's hydrocarbon,[1] 1,3,5-tris(diarylmethyl)benzene derivatives,[2] polyamine radical cations,[3] and several related molecules including covalently connected aminoxyl (nitroxide) moieties.[4–10] Moreover, it has been shown which spin states of organic molecules are achievable in excited states.[11,12]

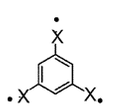

A X = C, N^+, ---NO

Another challenge in organic materials is to construct tunable devices that can be used as sensors. Constituents of such compounds should possess several stable states. For example, easily distinguishable redox stages and magnetic properties should be connected to different characteristic optical absorptions.[13–16] Although the magnetic features of a compound can be altered by the formation of excited states, their lifetimes are relatively short and cannot be tuned over a broad range. Another possibility for modifying magnetic properties is reversible electron transfer. This allows even control of the timescale of the magnetic response by choosing the appropriate "speed" of the redox process. Some examples have been described but radical-anion-based high-spin systems have only been reported in a few cases.[17–20]

In this contribution, we describe the properties of 1,3,5-tris(2,2-dicyanovinyl)benzene (**1**) and its trimethoxy derivative **2**. The redox behaviour of these two electron acceptors will be described as investigated by cyclic voltammetry (CV) and spectroelectrochemistry. The spin multiplicity and the structures of **1** and **2** after alkali-metal reduction will be characterised with the help of EPR experiments. In addition, quantum-mechanical calculations will assist to describe the electron distribution in the doublet-state radicals. Emphasis will be given to the correlation of UV–VIS spectra obtained by spectroelectrochemistry and SEOS[21] (simultaneous electron paramagnetic resonance–optical spectroscopy). Moreover, observations pointing to a specific radical anion–counterion interaction will be presented.

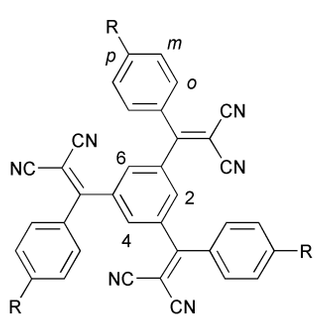

1 R = H
2 R = OCH_3

Experimental

Cyclic voltammetry and spectroelectrochemical measurements[22]

An undivided cell was used with a platinum disc as working electrode, a platinum counter electrode and a Ag/AgCl pseudo-reference electrode. The electrochemical measurements were carried out using computer-controlled electrochemical equipment consisting of an Amel System (Amel, Milano, Italy). The reversible oxidation signal of ferrocenium/ferrocene (Fc^+/Fc) or Ag/AgCl was used as internal reference. The solvents and the supporting electrolyte (0.1 M, tetrabutylammonium hexafluorophosphate, TBAHFP) were purified according to standard procedures. All measurements were carried out under a nitrogen atmosphere. The potentials are given *vs.* (Fc^+/Fc).

DOI: 10.1039/b202446b

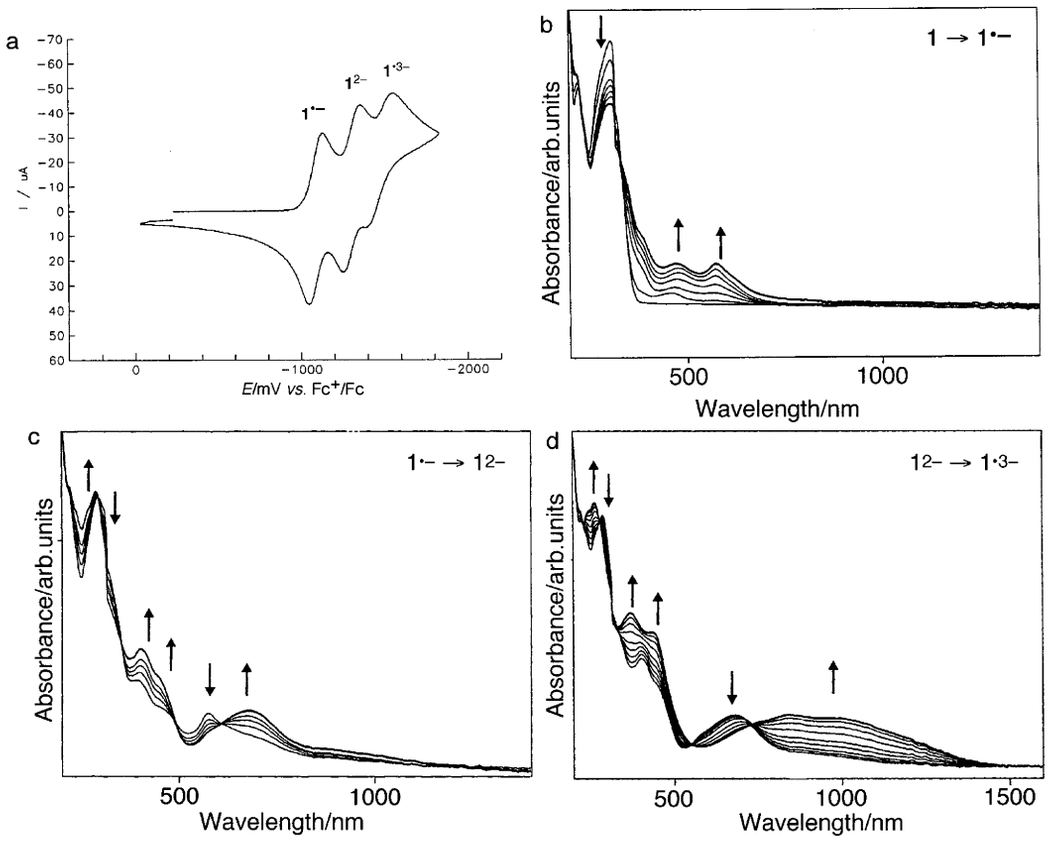

Fig. 1 a) Cyclic voltammogram of **1** (solvent, MeCN; supporting salt, tetrabutylammonium hexafluorophosphate; reference, Fc^+/Fc; scan rate, 250 mV s^{-1}); b) optical absorption spectrum recorded upon reduction of **1** to $\mathbf{1}^{\bullet-}$; c) optical absorption spectrum recorded upon reduction of $\mathbf{1}^{\bullet-}$ to $\mathbf{1}^{2-}$; d) optical absorption spectrum recorded upon reduction of $\mathbf{1}^{2-}$ to $\mathbf{1}^{3-}$. The arrows mark increasing and decreasing bands.

The solutions for the CV experiments were transferred by syringe techniques to the spectroelectrochemical cell. The spectra were recorded using a Perkin-Elmer LAMBDA 9 spectrophotometer equipped with a mirror configuration: mirror Pt-disk working electrode, Ag/AgCl pseudo-reference electrode and an Au counter electrode.

EPR spectra

For EPR measurements the samples were prepared under high vacuum. All solvents used (1,2-dimethoxyethane, THF, and 2-methyltetrahydrofuran) were refluxed over Na–K alloy and stored over Na–K alloy under high vacuum. The electron transfer reactions were performed by contact of the solutions of the parent compounds with a K-metal mirror. After each metal contact, the shape and the intensity of the EPR signals were checked over the temperature range between 273 and 130 K. EPR spectra were recorded on a Varian E9 and a Bruker ESP 300 spectrometer. The latter instrument served also for ENDOR and TRIPLE measurements. SEOS[21] (simultaneous EPR and optical spectra) were taken with a Varian E9 spectrometer equipped with an optical-transmission cavity (T102 mode). A TIDAS diode array (J&M, Aalen, Germany) optical spectrometer was attached to the optical outlets *via* quartz fibers.

The isotropic doublet EPR spectra were simulated with Winsim,[23] a public-domain program whereas the simulations of the spectra taken in rigid solution were performed using a home-made iterative program (Minuit-Simplex) based on a second-order perturbation algorithm with co-axial *g* and zero-field tensors.[24] The final adjustment was achieved with Simfonia (Bruker, Germany).[25] The line shapes for the simulations were Gaussian, with line widths between 0.8 and 1.2 mT.

Calculations of the anions in doublet states were performed with the Gaussian 94 package.[26] The geometries were optimised under the assumption of C_3 symmetry. For geometry optimisation and single-point determinations of the Fermi contacts, the UB3LYP/6-31G*//UHF/3-21G* protocol was used. This procedure generally leads to a rather efficient determination of isotropic hyperfine coupling constants (hfcs).[27]

Results and discussion

Redox potentials and UV–VIS spectra

The cyclic voltammogram of **1** indicates three clearly distinguishable, reversible (or *quasi*-reversible) redox steps. The first step at −1.09 V *vs.* Fc^+/Fc (peak separation, ΔE_{PP} = 80 mV) represents the reduction of parent **1** to its radical anion ($\mathbf{1}^{\bullet-}$), whereas the second ($E_{½}$ = −1.31 V; ΔE_{PP} = 100 mV) and the third ($E_{½}$ = −1.48 V; ΔE_{PP} = 150 mV) steps mirror the formation of the di- ($\mathbf{1}^{2-}$) and the trianion ($\mathbf{1}^{3\bullet-}$), respectively (Fig. 1a). The optical absorption spectra recorded during the reduction are represented in Fig. 1b–d. The dominant absorption of parent **1** at 302 nm decreases upon the uptake of the first electron whereas two sharp characteristic bands for $\mathbf{1}^{\bullet-}$ emerge at 473 and 574 nm (Fig. 1b). Further reduction to the dianion ($\mathbf{1}^{2-}$) is accompanied by novel absorptions at 290, 403, 454, and 677 nm while the bands attributed to the radical anion disappear (Fig. 1c). The most remarkable change in going from $\mathbf{1}^{2-}$ to $\mathbf{1}^{3\bullet-}$ is the development of a broad band at 900 nm (range 600–1400 nm); moreover, absorptions at 442, 371, and 265 nm can be associated with $\mathbf{1}^{3-}$ (Fig. 1d).

A similar reactivity is found for methoxy derivative **2**. The first reversible electron transfer ($\rightarrow\mathbf{2}^{\bullet-}$) occurs at $E_{½}$ = −1.34 V *vs.* Fc^+/Fc (ΔE_{PP} = 80 mV), the second ($\rightarrow\mathbf{2}^{2-}$) at −1.56 V ($\Delta E_{PP}$ = 80 mV) and the third ($\rightarrow\mathbf{2}^{3\bullet-}$) at −1.81 V ($\Delta E_{PP}$ = 100 mV). The distinctive absorption bands for the four redox stages found for **2** are summarised in Table 1.

Table 1 Redox potentials and absorption bands of the four redox stages of **1** and **2**

Step	Potential *vs.* Fc^+/Fc/V	Optical absorption bands/nm				
1		302				
$\mathbf{1} \longrightarrow \mathbf{1}^{\bullet -}$	−1.09	473	574			
$\mathbf{1}^{\bullet -} \longrightarrow \mathbf{1}^{2-}$	−1.31	290	403	454	677	
$\mathbf{1}^{2-} \longrightarrow \mathbf{1}^{3\bullet -}$	−1.48	265	371	442	900 (br)	
2		238	276	345		
$\mathbf{2} \longrightarrow \mathbf{2}^{\bullet -}$	−1.34	230	282	477	570	1400
$\mathbf{2}^{\bullet -} \longrightarrow \mathbf{2}^{2-}$	−1.56	226	297	430	700	
$\mathbf{2}^{2-} \longrightarrow \mathbf{2}^{3\bullet -}$	−1.81	273	448	1100		

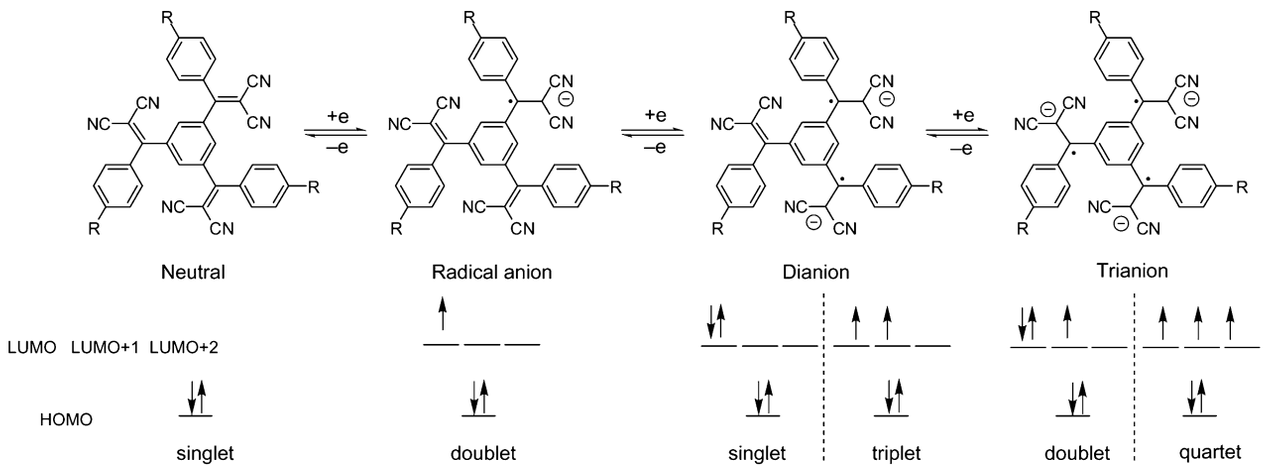

Scheme 1

Magnetic characteristics

According to molecular-orbital calculations, the LUMO, the LUMO+1, and the LUMO+2 of **1** and **2** are almost degenerate. Accordingly, the uptake of more than one electron can lead to diverse magnetic stages. The first reduction produces a doublet radical anion which can be characterised by the EPR data derived from the fluid-solution EPR spectra. The addition of the second electron either yields a diamagnetic singlet or a paramagnetic triplet whereas the trianion can either form a doublet or a quartet state (Scheme 1). For the interpretation of the EPR spectra of these species one has to keep in mind not only the two spin multiplicities which are connected with one single redox stage but also that additional stages (*e.g.* dianion/trianion) may be present (coexisting in equilibrium).

Fluid-solution doublet EPR spectra

Potassium reduction of **1** and **2** in THF or 2-methyltetrahydrofuran led to well-defined EPR and ENDOR spectra. Their shape did not show any dependence on the nature of the solvent. The simulations of the EPR spectra ascribed to $\mathbf{1}^{\bullet -}$–K^+ and $\mathbf{2}^{\bullet -}$–K^+ were accomplished with the isotropic proton hyperfine coupling constants (^{1}H hfcs) detected by ENDOR and ^{14}N hfcs determined by a fitting procedure. The EPR spectrum obtained after a short (*ca.* 10 s) contact of the THF solution of **1** with the potassium mirror is shown in Fig. 2a. The four-line pattern (intensity ratios 1 : 3 : 3 : 1) is in line with three equivalent protons (within the hyperfine timescale). The corresponding ^{1}H hfc of 0.35 (3 H) mT is also clearly resolved in the ENDOR spectrum (Fig. 2b) showing two additional ^{1}H hfcs of 0.06 (9 H) and 0.02 (6 H) mT which are not distinguishable in the EPR spectrum. In addition, a ^{14}N hfc of approximately 0.05 (6 N) mT can be deduced from the EPR simulations. These experimental values are in very good agreement with their calculated counterparts for $\mathbf{1}^{\bullet -}$ (Table 2).

The SEOS spectrum (Fig. 2c) indicates bands at 401, 423, 435, 489, 509, 550, 596, and 705 nm. According to the spectroelectrochemical measurements, these bands reveal the presence of a mixture of the dianion ($\mathbf{1}^{2-}$) and the radical anion ($\mathbf{1}^{\bullet -}$) in solution (*cf.* Table 1).

Further contact with the metal mirror leads to a decrease of the primary EPR signal. After *ca.* 12 h of metal contact at 193 K, a novel EPR spectrum emerges (Fig. 3a). This EPR signal (width *ca.* 2.2 mT) is well resolved and the corresponding ENDOR spectrum (Fig. 3b) exhibits ^{1}H hfcs of 0.21 (9 H), 0.01 (6 H), and 0.03 (3 H) mT. Together with a ^{14}N hfc of 0.10 (6 N) mT a perfect match between the experimental and the simulated spectrum is achieved (Fig. 3). In accord with the quantum-mechanical calculations, these data point to the presence of radical trianion $\mathbf{3}^{\bullet 3-}$ in which the spin and the charge are evenly delocalised in the peripheral phenyl and the dicyanovinyl substituents on the hyperfine timescale. The SEOS-electronic spectrum (broad absorptions between 400 and 650 nm, a superposition of bands attributable to the di- and trianion Table 1) corroborates the assignment of the spectra shown in Fig. 3 to the doublet trianion $\mathbf{1}^{\bullet 3-}$.

Virtually the same EPR spectrum as for $\mathbf{1}^{\bullet -}$ is obtained after the first reduction of **2**. The quartet has an hfc of 0.35 mT and the ^{1}H hfcs discernible in the ENDOR spectrum are 0.03 and 0.06 mT (Table 2). Prolonged contact of a solution of **2** in THF or 2-methyltetrahydrofuran did not yield any spectra pointing to products of a subsequent doublet-state redox stage.

Structure of the doublet-state radical ions

The hfcs of 0.35 and 0.37 mT in $\mathbf{1}^{\bullet -}$ and $\mathbf{2}^{\bullet -}$ attributable to three equivalent protons demonstrate that the dominant portion of the spin is mainly concentrated inside the central trisubstituted benzene ring. This is borne out by the almost identical EPR spectra ascribed to $\mathbf{1}^{\bullet -}$–K^+ and $\mathbf{2}^{\bullet -}$–K^+. The *para*-methoxy groups in the phenyl substituents have no influence on the hyperfine structure and the ^{14}N hfcs are negligibly small, *i.e.* there is almost no delocalisation of spin into the aryl and the cyanovinyl substituents. The overall threefold symmetry is preserved in the radical anions on the hyperfine timescale as substantiated by very good agreement with the calculated values (Table 2).

Table 2 Data from the EPR, ENDOR, and SEOS spectra assigned to $\mathbf{1}^{\bullet-}$–K^+, $\mathbf{1}^{3\bullet-}$–3 K^+, and $\mathbf{2}^{\bullet-}$–K^+, together with hfcs calculated (UB3LYP/6-31G*//UHF/3-21G*) for $\mathbf{1}^{\bullet-}$–K^+ and $\mathbf{1}^{3\bullet-}$–3 K^+

Position[a]	2,4,6	*o*/*p*	*m*	N	*g* Factor	SEOS bands/nm
No. of nuclei	3 H	9 H (**2**: 6 H)	6 H	6 N		
$\mathbf{1}^{\bullet-}$ (exp.)	0.35	0.06	0.03	>0.05	2.0018	395, 492, 584
$\mathbf{2}^{\bullet-}$ (exp.)	0.37	0.05	0.03		2.0018	493, 587, 688 (sh)
$\mathbf{1}^{\bullet-}$ (calc.)	−0.45	−0.06	+0.03			
$\mathbf{1}^{3\bullet-}$ (exp.)	0.03	0.21	0.01	0.10	2.0017	466, 639
$\mathbf{1}^{3\bullet-}$ (calc.)	−0.07	−0.07	+0.04	+0.04		

[a] The positions to which the hfcs (columns 2–4, all values in mT) are attributed are indicated in the formula of **1**.

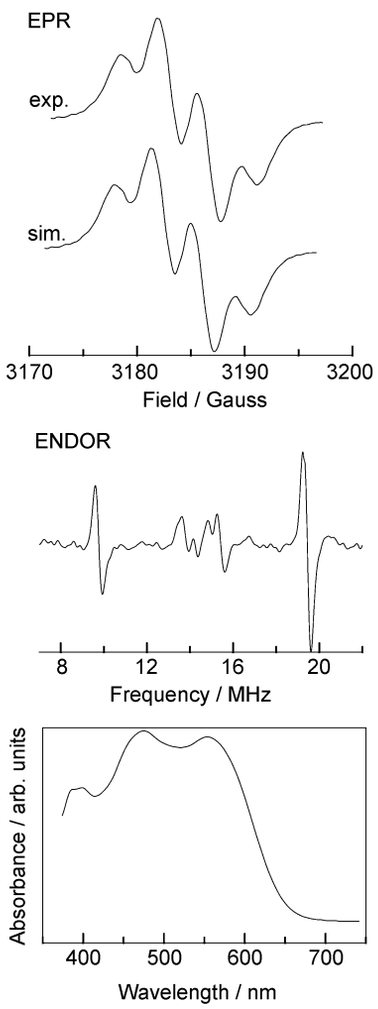

Fig. 2 a) EPR; b) ENDOR; c) SEOS spectra obtained after a short contact of a THF solution of **1** with a K-metal mirror.

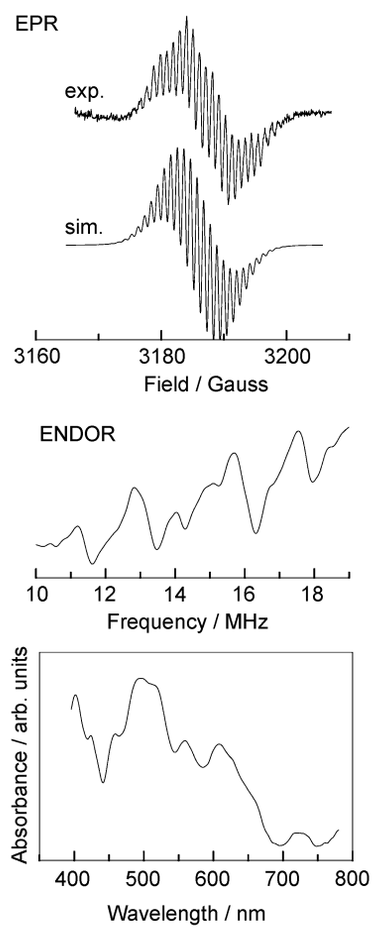

Fig. 3 a) EPR; b) ENDOR; c) SEOS spectra obtained after exhaustive reduction of a THF solution of **1** with a K-metal mirror.

This spin distribution is reversed in the radical trianion $\mathbf{1}^{3\bullet-}$ to which we attribute the EPR spectra shown in Fig 3. The resolved EPR splittings are due the interaction of nine apparently equivalent protons and two equivalent nitrogen nuclei with one unpaired electron. These multiplicities reflect a considerable amount of spin population in the phenyl and cyano groups of $\mathbf{1}^{3\bullet-}$. In harmony with the predicted values, no significant amount of spin resides in the central moiety (Table 2). Such a spin and charge distribution certainly leads to the stabilization of the highly charged species and enhances ion pairing.

EPR spectra of high-spin states in rigid solution

What are the highest paramagnetic stages achievable for the anions of **1** and **2**? Whereas the fluid-solution EPR spectra serve as tools to mirror the structure of the doublet states of **1** and **2** attainable by electron transfer, solid-state EPR spectra allow insight into the structures of electron-spin states with $S > ½$. To produce the higher spin states, exhaustive reduction with a K-mirror of **1** and **2** was carried out (solvents, THF and 2-methyltetrahydrofuran). The solutions were frozen, and EPR spectra were taken over the temperature range between 100 and 150 K.

In Fig. 4a the EPR spectrum of **1** in 2-methyltetrahydrofuran (after exhaustive K-reduction) at 103 K is shown. It consists of superimposed signals in the region of $g = 2$ ($\Delta m_s = 1$). The simulation of this EPR signal can only be accomplished if a mixture of a two-spin system in a triplet state ($S = 1$, Fig. 4c) and a three-spin system in a quartet state ($S = \frac{3}{2}$, Fig. 4d), with different parameters for both species, is taken into account. The simulated spectrum is presented in Fig. 4b. We were unable to detect the half-field signal due to the greatly reduced intensity of this transition in comparison with the $\Delta m_s = 1$ transition because of a small zero-field splitting (see below).[1,28]

As indicated in Scheme 1, only a singular combination of redox stages can lead to the experimental EPR signal: The triplet state can only be based on the dianion, $\mathbf{1}^{2-}$–2 K^+ whereas the quartet state has to originate from the trianion $\mathbf{1}^{3\bullet-}$–3 K^+.

Table 3 EPR data assigned to the triplet dianions of $\mathbf{1}^{2-}$ and $\mathbf{2}^{2-}$ and the quartet trianion $\mathbf{1}^{3\bullet-}$

	Dianion: triplet state		Trianion: quartet state
	D'/cm^{-1}	E'/cm^{-1}	D'/cm^{-1}
1	0.0102	0.0014	0.0033
2	0.0104	0.0018	—

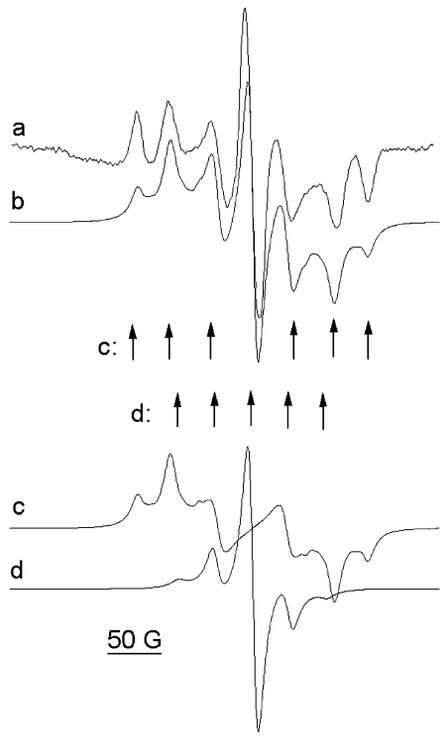

Fig. 4 a) EPR spectrum of **1** in K–2-methyltetrahydrofuran, at 103 K; b) simulation; c) simulation of the triplet-state component; d) simulation of the quartet-state component. The arrows indicate where the triplet-state and the quartet-state lines can be found in the experimental spectrum.

The observed $D' = |D|/hc$ and $E' = |E|/hc$ values for the triplet state of $\mathbf{1}^{2-}$–2 K^+ are 0.0102 and 0.0014 cm^{-1}, respectively (Fig. 4c, Table 3). The D' value is a bit smaller than that for the *meta*-substituted hydrocarbon **3** (0.011 cm^{-1}), but much bigger than that for 1,3,5-tris(diphenylmethyl)benzene (**5**),[2] or **4**[1] with D' = 0.0068 and 0.0064 cm^{-1}, respectively; this is presumably due to a less extended spin delocalisation into the phenyl groups of $\mathbf{1}^{2-}$–2 K^+ (and analogously $\mathbf{2}^{2-}$–2 K^+).

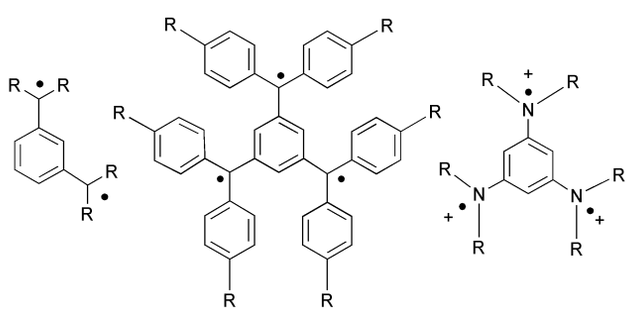

Regarding the formal 3-fold symmetry it may be surprising that the E' values of 0.0014 and 0.0018 cm^{-1} for the two dianions have to be taken into account indicating a deviation from axial symmetry.[19] Here, a conformational change and/or a close association with the counterions in the solid state could easily account for the decrease of symmetry. This E' value is similar to that of dicationic *N*,*N*,*N*′,*N*′,*N*″,*N*″-hexakis-(*p*-methoxyphenyl)-1,3,5-triaminobenzene (**7**, E' = 0.0011 cm^{-1}) which formally also has three-fold symmetry.[3] An additional factor, the electron correlation, must be considered for a triplet state, which tends to increase the electron–electron separation and may therefore favour a distorted structure. The remarkable intensity of the central signal and the existence of the outer lines observed upon exhaustive reduction of **1** (Fig. 4a) are characteristic of a quartet state radical with a zero-field parameter D' of 0.0033 cm^{-1} (Fig. 4d). This value is smaller than those of 0.0049 cm^{-1} for 1,3,5-tris(diphenylmethyl)benzene (**5**)[2] 0.0046 cm^{-1} for **7**,[3] or 0.0041 cm^{-1} for **3**,[29] and correlates with a larger distance between the unpaired electrons in **1**.[30] At the same time, this value is greater than 0.0026 cm^{-1}, corresponding to published values for **6**.[4]

The EPR spectrum of **2** in K–THF at 143 K is shown in Fig. 5a. For its successful simulation (Fig. 5b) two paramagnetic

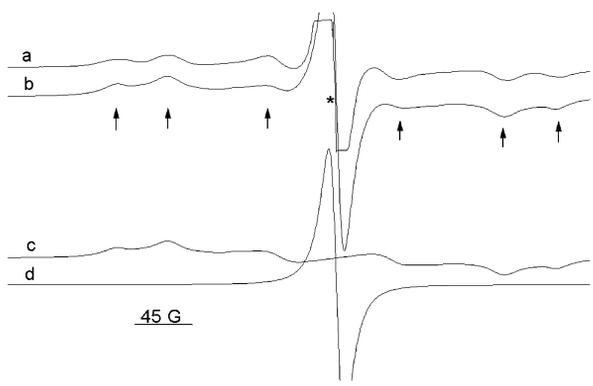

Fig. 5 a) EPR spectrum of **2** in K–THF, at 143 K; b) simulation; c) simulation of the triplet-state component; d) simulation of the doublet-state component. The arrows and the asterisk indicate where the triplet-state and the doublet-state line, respectively, can be found in the experimental spectrum.

species, *i.e.*, a triplet-state radical (S = 1) and a doublet-state radical (S = ½), have to be considered. According to Scheme 1 these states can originate from the radical anion or the trianion as the doublet component with the dianion forming the triplet. Because we were not able to obtain a fluid-solution EPR signal attributable to the trianion of **2** in the doublet state, we ascribe the doublet component to $\mathbf{2}^{\bullet-}$–K^+.

The zero-field parameters D' and E' used for the simulation of the EPR signal of the triplet-state anion $\mathbf{2}^{2-}$–2 K^+ are 0.0104 and 0.0018 cm^{-1} (Fig. 5c), respectively, match the zero-field parameters of $\mathbf{1}^{2-}$–2 K^+. The similarity reveals that in both cases almost identical triplet states are formed and that the methoxy substituent does not alter the character of the magnetic electron–electron dipolar interactions.

In contrast to the frozen-solution spectra obtained after exhaustive reduction of **1**, the central peak is very intense for **2** and it cannot be simulated by considering a quartet-state spectrum, without drastically modifying the intensity of the outer lines (Fig. 5a). Thus, the second EPR spectrum has to be attributed to a doublet-state radical (Fig. 5d).

As for compound **1**, the half-field signal, corresponding to the $\Delta m_s = 2$ transition, was not observed.

Structure of the high-spin-state radical ions

For both triplet-state radicals, the interspin distance, r, between two unpaired electrons can be estimated from the D' values[31] and allows insight into the molecular structure of the paramagnetic biradical. We assume that D' is due only to dipolar interaction with no contribution from anisotropic exchange and that E' can be neglected. In this case the following equation can be applied:[32]

$$D' = 1.39 \times 10^4 \, (g/r^3)$$

where D' has to be converted to mT and r is in Å. In the case of $\mathbf{1}^{2-}$ we obtain an r value of 6.4 Å. The same calculation for $\mathbf{2}^{2-}$ yields a similar interspin distance of 6.30 Å. Both values are in very good agreement with the calculated distance between two dicyanovinyl moieties (6.5 Å) and reveal that the two electrons are not essentially delocalized within the molecular π system.

Conclusions

High-spin states are formed by reduction of electron acceptors **1** and **2**. Although the cyclic voltammograms indicate distinct redox steps for the transfer of one, two and three electrons, equilibrium populations between two adjacent redox stages are established in the solutions of K-reduced **1** and **2**. This points to differences between the conditions within the thin diffusion layer around the working electrode in the electrochemical experiment and the bulk solution observed by EPR. Moreover, a closer association between the alkali-metal cation and the negatively charged radical may lead to a shift in the reduction potentials and cause the presence of a number of redox stages in equilibrium.

It is interesting to note that the high-spin states of the anions generated from **1** could only be detected in 2-methyltetrahydrofuran whereas the triplet state of $\mathbf{2}^{2-}$–2 K^+ was exclusively discernible in THF. This illustrates that specific solute–solvent–counterion interactions are able to influence the properties of the anionic high-spin states. Such behaviour was established for the triplet states of the dianion of 1,3,5-triphenylbenzene where specific ion-pairing led to either triplet or singlet ground states together with symmetry alternations.[19] A symmetry decrease reported for the radical cations also points to association phenomena.[33,34]

Unfortunately temperature variation in the range between 100 and 150 K did not yield significant alternations of the line intensities, thus impeding determination of whether the high-spin states mirrored by the EPR signals are the ground or thermally populated states of the corresponding anions. Moreover, it would be interesting to estimate the electronic coupling J.

Remarkably the formation of the anionic high-spin states of **2** and, particularly, **1** affords relatively low potentials (Table 1). This thermodynamic stability makes the cyanovinyl-substituted benzenes ideal candidates for further structural modifications and studies.

Acknowledgements

G.G. and C.P. thank the Swiss National Science Foundation and Ciba Speciality Chemicals Inc., Basel, for financial support.

References

1 C. G. Luckhurst and G. F. Pedulli, *J. Chem. Soc.*, 1971, 329.
2 W. Wilker, G. Kothe and H. Zimmermann, *Chem. Ber.*, 1975, **108**, 2124.
3 K. R. Stickley and S. C. Blackstock, *Tetrahedron Lett.*, 1995, **36**, 1585.
4 G. Kothe, F. A. Neugebauer and H. Zimmermann, *Angew. Chem., Int. Ed. Engl.*, 1972, **11**, 830.
5 H. Iwamura, *J. Phys. Org. Chem.*, 1998, **11**, 299.
6 H. Iwamura and N. Koga, *Pure Appl. Chem.*, 1999, **71**, 231.
7 O. Kahn, *Actual. Chim.*, 1996, 62.
8 J. S. Miller and A. J. Epstein, *Adv. Chem. Ser.*, 1995, **245**, 161.
9 H. O. Stumpf, L. Ouahab, Y. Pei, P. Bergerat and O. Kahn, *J. Am. Chem. Soc.*, 1994, **116**, 3866.
10 M. Tanaka, K. Matsuda, T. Itoh and H. Iwamura, *J. Am. Chem. Soc.*, 1998, **120**, 7168.
11 Y. Teki, S. Miyamoto, K. Iimura, M. Nakatsuji and Y. Miura, *J. Am. Chem. Soc.*, 2000, **122**, 984.
12 Y. Teki, S. Miyamoto, M. Nakatsuji and Y. Miura, *J. Am. Chem. Soc.*, 2001, **123**, 294.
13 C. Lambert, G. Nöll, E. Schmälzlin, K. Meerholz and C. Bräuchle, *Chem. Eur. J.*, 1998, **4**, 2129.
14 A. Behrendt, C. G. Screttas, D. Bethell, O. Schiemann and B. R. Steele, *J. Chem. Soc., Perkin Trans. 2*, 1998, 2039.
15 T. Nakamura, T. Momose, T. Shida, K. Sato, S. Nakazawa, T. Kinoshita, T. Takui, K. Itoh, T. Okuno, A. Izuoka and T. Sugawara, *J. Am. Chem. Soc.*, 1996, **118**, 8684.
16 M. C. R. L. R. Lazana, M. L. T. M. B. Franco and M. C. B. L. Shohoji, *J. Chem. Res., Synop.*, 1996, 48.
17 M. Baumgarten, *Acta Chem. Scand.*, 1997, **51**, 193.
18 M. Baumgarten, U. Müller, A. Bohnen and K. Müllen, *Angew. Chem., Int. Ed. Engl.*, 1992, **31**, 448.
19 J. A. M. Broekhoven, J. L. Sommerdijk and E. de Boer, *Mol. Phys.*, 1971, **20**, 993.
20 J. Sedo, D. Ruiz, J. Vidal-Gancedo, C. Rovira, J. Bonvoisin, J. P. Launay and J. Veciana, *Adv. Mater.*, 1996, **8**, 748.
21 G. Gescheidt, *Rev. Sci. Instrum.*, 1994, **65**, 2145.
22 M. Büschel, C. Stadler, C. Lambert, M. Beck and J. Daub, *J. Electroanal. Chem.*, 2000, **484**, 24.
23 D. R. Duling, *PEST Winsim*, NIEHS, Research Triangle Park, NC, USA, 1995.
24 E. Wasserman, L. C. Snyder and W. A. Yager, *J. Chem. Phys.*, 1964, **41**, 1763.
25 Bruker, *Simfonia*, Rheinstetten, 1996.
26 M. J. Frisch, G. W. Trucks, H. B. Schlegel, P. M. W. Gill, B. G. Johnson, M. A. Robb, J. R. Cheeseman, T. Keith, G. A. Petersson, J. A. Montgomery, K. Raghavachari, M. A. Al-Laham, V. G. Zakrzewski, J. V. Ortiz, J. B. Foresman, C. Y. Peng, P. Y. Ayala, W. Chen, M. W. Wong, J. L. Andres, E. S. Replogle, R. Gomperts, R. L. Martin, D. J. Fox, J. S. Binkley, D. J. Defrees, J. Baker, J. P. Stewart, M. Head-Gordon, C. Gonzalez and J. A. Pople, Gaussian 94, Revision B.3, Gaussian, Inc., Pittsburgh PA, 1995.
27 R. Batra, B. Giese, M. Spichty, G. Gescheidt and K. N. Houk, *J. Phys. Chem.*, 1996, **100**, 18371.
28 A. de Meijere, F. Gerson, B. König, O. Reiser and T. Wellauer, *J. Am. Chem. Soc.*, 1990, **112**, 6827.
29 G. Kothe and H. Zimmermann, *Tetrahedron*, 1973, **29**, 2305.
30 A. Calder, A. R. Forrester, P. G. James and G. R. Luckhurst, *J. Am. Chem. Soc.*, 1969, **91**, 3724.
31 G. R. Luckhurst, in *Spin Labelling: Theory and Applications*, ed. L. J. Berliner, Academic Press, New York, 1976, p. 149.
32 S. E. Eaton, K. M. More, B. M. Sawant and G. R. Eaton, *J. Am. Chem. Soc.*, 1983, **105**, 6560.
33 K. R. Stickley, T. D. Selby and S. C. Blackstock, *J. Org. Chem.*, 1997, **62**, 448.
34 K. R. Stickley and S. C. Blackstock, *J. Am. Chem. Soc.*, 1994, **116**, 11576.